N_2 Desorption in the Decomposition of Adsorbed N_2O on Rh(110)

Suwen Liu,[†] Hideyuki Horino,[‡] Anton Kokalj,[§] Izabela Rzeźnicka,[‡] Kenji Imamura,[‡] Yunsheng Ma,[†] Ivan Kobal,[§] Yuichi Ohno,[†] Atsuko Hiratsuka,[†] and Tatsuo Matsushima*[,†]

Catalysis Research Center, Hokkaido University, Sapporo 001-0021, Japan, Graduate School of Environmental Earth Science, Hokkaido University, Sapporo 060-0810, Japan, and Jozef Stefan Institute, 1000 Ljubljana, Slovenia

Received: October 15, 2003

The decomposition of N_2O(a) was studied on Rh(110) at 95−200 K through the analysis of the angular distributions of desorbing N_2 by means of angle-resolved thermal desorption. N_2O(a) was highly decomposed during the heating procedures, emitting N_2(g) and releasing O(a). N_2 desorption showed four peaks, at 105−110 K (β_4-N_2), 120−130 K (β_3-N_2), 140−150 K (β_2-N_2), and 160−165 K (β_1-N_2). The appearance of each peak was sensitive to annealing after oxygen adsorption and also to the amount of N_2O exposure. The β_1-N_2 peak was major at low N_2O exposures and showed a cosine distribution. On the other hand, β_2-N_2 and β_3-N_2 on an oxygen-modified surface revealed inclined and sharp collimation at around 30° off the surface normal in the plane along the [001] direction, whereas β_4-N_2 on a clean surface collimated at around 70° off the surface normal, close to the [001] direction. An inclined or surface-parallel form of adsorbed N_2O was proposed as the precursor for inclined N_2 desorption.

I. Introduction

N_2O decomposition on rhodium surfaces has attracted much attention in the catalytic removal of nitrogen oxides in exhaust gases since rhodium is one of the best catalysts for this process and N_2O is the main byproduct in NO decomposition.[1] Furthermore, N_2O itself is harmful and yields a remarkable greenhouse effect. The NO decomposition mechanism via the N_2O(a) intermediate has been frequently proposed on this metal[2] to explain the concomitant desorption of N_2O, NO, and N_2. However, the discussion is still controversial, except for the preference of the associative desorption of $2N(a) \rightarrow N_2(g)$ at high temperatures. Our group recently confirmed a large contribution to N_2 emission from the N_2O(a) intermediate in both NO and N_2O decompositions over Pd(110) from the close similarity in the angular and velocity distributions of desorbing N_2.[3] Desorbing N_2 is highly concentrated in the plane along the [001] direction with a hyper-thermal energy and collimates at 43−50° off the surface normal.[4,5] Such a peculiar N_2 emission is useful to examine the reaction mechanism because the combinative desorption of N(a) shows normally directed emission.[6,7]

This paper delivers the first report of N_2O(a) decomposition on clean and oxygen-modified Rh(110) in the range of the surface temperature of 95−200 K. The decomposition yielded four N_2 desorption peaks, at 105−110 K (β_4-N_2), 120−130 K (β_3-N_2), 140−150 K (β_2-N_2), and 160−165 K (β_1-N_2). The β_1-N_2 peak showed a cosine distribution. On the oxygen-modified surface, β_2-N_2 and β_3-N_2 revealed a very sharp collimation at around 30° off the surface normal in the plane along the [001] direction, whereas β_4-N_2 on the clean surface collimated at around 70° off the surface normal.

It is well-known that NO dissociation on Rh(110) is retarded by adsorbed oxygen.[8] However, NO is easily decomposed on it although the surface does not seem to be free from oxygen because complete removal of oxygen from this surface is very difficult.[9] This suggests the presence of different kinds of surface oxygen which affect the dissociation of NO. Rh(110) is reconstructed into the (1 × 2) missing-row form by being heated above 500 K after oxygen adsorption. Scanning tunneling microscopy (STM) work indicates that oxygen at this stage forms O−Rh−O−Rh zigzag chains extending along the [1$\bar{1}$0] direction.[10] Such oxygen prevents N_2O from dissociating because the local oxygen coverage is a 0.5 monolayer, which is enough to completely suppress the dissociation. At much lower oxygen coverage, N_2O is decomposed, but the angular distribution of desorbing product N_2 has not been examined. Our preliminary report showed that the inclined N_2 desorption in N_2O decomposition on clean Rh(110)(1 × 1) was very different from the results on Pd(110).[4,5,11]

Belton et al. could not confirm, in their isotopic thermal desorption spectroscopy (TDS) work, that N_2O produced on Rh(111) yielded N_2.[12] Zaera and Gopinath reported that the replacement of surface ^{14}N(a) by ^{15}N(a) upon shifting from ^{14}NO(g) to ^{15}NO(g) in a steady-state CO + NO reaction yielded $^{15}N_2$ and $^{14}N^{15}N$ in large amounts.[13] This result indicates that such an isotope method has difficulty in differentiating between the two N(a) removal processes mentioned above in the course of the catalyzed reaction.

II. Experimental Section

Two UHV apparatuses were used. One had low-energy electron diffraction (LEED) and X-ray photoelectron spectroscopy (XPS) facilities, and the other had three chambers for angle-resolved thermal desorption spectroscopy (AR-TDS).[14] These chambers were separately evacuated by individual ion pumps. The reaction chamber was equipped with LEED-Auger electron spectroscopy (AES), an Ar^+ gun, a quadruple mass

* Corresponding author. Fax: +81-11-706-9110. E-mail: tatmatsu@cat.hokudai.ac.jp.
[†] Catalysis Research Center, Hokkaido University.
[‡] Graduate School of Environmental Earth Science, Hokkaido University.
[§] Jozef Stefan Institute.

10.1021/jp037130p CCC: $27.50
Published on Web 02/27/2004

spectrometer (QMS) for angle-integrated (AI) analysis, and a gas-handling system. The collimation chamber had a slit on both ends. The analyzer chamber had another QMS for angle-resolved (AR) desorption measurements. A Rh(110) crystal was set on the top of a rotatable manipulator to change the desorption angle (θ; the polar angle) in the normally directed plane along the [001] direction. It was cleaned by standard cycles of Ar^+ sputtering, oxygen treatment, and annealing to 1100 or 1200 K as described in the Results section. The surface was exposed to $^{15}N_2O$ through a gas doser when the surface temperature was at around 95 K and then was heated in most cases at a rate of 2 K s^{-1} below 250 K and 8 K s^{-1} above it. On the other hand, the heating rate of 0.6 K s^{-1} was used on the clean surface. The actual pressure of N_2O at the sample surface was 6.4 times higher than the value at the pressure gauge position.[5] For CO and oxygen exposures, a doser was not used.

The fragmentation of N_2O was separately examined in each mass spectrometer under a constant flow of this species. The AI-signal due to the mass number 30 ($^{15}N_2^+$) was estimated to involve a contribution of 70% of the $^{15}N_2O$ signal in the AI form. On the other hand, about three times as much as the AR-N_2O signal contributed to the AR-N_2 signal, i.e., roughly 75% of the N_2O that entered the analyzer ionizer was decomposed. The correction based on these fragmentations was significant over a wide range of N_2O exposures on the oxygen-modified surface. This large fragmentation in the analyzer is due to the use of a compact box-type ionizer. Hereafter, isotope ^{15}N is simply designated as N in the text.

It was not easy to reproduce the definite initial surface condition by only annealing after oxygen or N_2O exposure because the amount of remaining oxygen depended on the interval and temperature of annealing. A clean surface was obtained after 5 min or longer heating at 1200 K; this was shown by the clear (1 × 1) LEED pattern and the lack of a TDS peak of oxygen as well as the lack of inclined N_2 desorption at $\theta = 30°$, as described in the next sections. However, the sample was mostly flashed to 1100 K after each run to avoid damaging the alumel−cromel thermocouple. This flashing temperature was not high enough to completely remove the surface oxygen.[9] The amount of remaining surface oxygen was less than about 20% of the saturation level, as judged from the TDS of oxygen.

III. Results

A. LEED Studies. The LEED observations showed a strong (1 × 1) structure with a very weak (2 × 1) form after high N_2O exposures at 90 K. This pattern was kept until the surface was heated to 190 K. Hence, the surface was not further reconstructed during N_2O decomposition completed below 160 K. This structure was converted into intense (1 × 3) or (1 × 2) spots after heating above 400 K. These super structures are due to the missing row induced by oxygen adsorption.[8] The surface showed the (1 × 3)-O lattice after flashing to 1100 K. This surface was used as the oxygen-modified surface. The remaining oxygen at this stage was not necessarily on the surface because the resultant surface already showed activity for N_2O decomposition although less than this level of adsorbed oxygen (without annealing after oxygen exposure) completely prevented N_2O from decomposing. This lattice disappeared by flashing above 1150 K. The (1 × 1) pattern was already clear after heating at 1100 K for 5 min, or flashing to 1200 K without being kept at this temperature. However, the subsequent desorption phenomena still involved the contribution from the oxygen-modified area as described below. For the preparation of clean Rh(110), the surface was heated at 1200 K for 5 min. No carbon contamination was found after this preparation by LEED and XPS, probably because the surface was once covered by oxygen and heated in each TDS procedure.

B. Clean Rh(110). The surface was initially cleaned by heating for 5 min at 1200 K. After N_2O exposures at 95 K, N_2O(a) was highly dissociated in the subsequent heating. N_2O desorption was noticed only above exposures yielding near-saturation of N_2 desorption. N_2O desorption peaked at around 115 K and was completed at around 130 K. Its peak area in the AI-form was always below 10% of that of N_2. Here, the N_2O coverage, Θ_{N_2O}, was defined as the AI-TDS peak area relative to the sum of ($N_2 + N_2O$) at saturation of N_2 desorption. This is actually consistent with the coverage definition on the oxygen-modified surface described below. About 1.9 L (Langmuir = 1 × 10^{-6} Torr s) N_2O was exposed until N_2 saturation. This is much more than that on the oxygen-modified surface in the following section. This suggests significant dissociation of N_2O at 95 K on the clean surface[15] and the product N_2 partly leaves the surface before the subsequent TDS procedure. N_2O dissociation behavior on clean Rh(110) must be studied at much lower adsorption temperatures.

N_2 desorption started at around 95 K and two peaks first appeared at 110 K (β_4-N_2) and 167 K (β_1-N_2) (Figure 1a). Significant signals were observed between the above two peaks, suggesting the presence of additional peaks. The β_4-N_2 signal was enhanced in the AR form around $\theta = 70°$ as compared with that at $\theta = 0°$ (Figure 1b). For the angular distribution analysis, the peak temperature and peak height of each N_2 desorption were determined by curve fitting, in which a Gaussian form with fixed values for its peak position and half-width was assumed for each peak[5] (Figures 1a and 1b). The remaining signal, after subtraction of β_1-N_2 and β_4-N_2, seemed to involve two peaks at around 130 and 145 K, and the signal is called (β_2-N_2 + β_3-N_2). This component was highly enhanced at high N_2O exposures and overlapped with the others. The formation of β_1-N_2 at around 167 K was major from low exposures and showed a simple cosine distribution (Figure 1c). The signal of β_4-N_2 was maximized at around $\theta = \pm 70°$ and approximated as $\cos^{15}(\theta + 70) + \cos^{15}(\theta - 70)$ (Figure 1d). The (β_2-N_2 + β_3-N_2) signal followed an angle dependence similar to that of β_4-N_2. At coverages higher than about 50% of saturation, it became difficult to examine the angular distributions because of the large overlapping of peaks.

C. Oxygen-Modified Rh(110). *C.1. N_2O Desorption and Its Angular Distribution.* Before each N_2O exposure, the surface was preexposed to N_2O in the same amount as that in the subsequent dosage and flashed to 1100 K in every TDS procedure. This procedure was requisite for reproducible data. The resultant surface still involved oxygen, but in a form different from that before annealing. For this reason, the surface was called the oxygen-modified surface. The branching ratio of N_2 to N_2O in the subsequent heating decreased on this surface because N_2O desorption became noticeable above around 60% of N_2 saturation. The surface oxygen content was much less than 20% because N_2O(a) was still highly decomposed in the subsequent heating. In fact, as described in Section D, a smaller amount of surface oxygen was enough to mostly suppress the N_2O decomposition when the surface was used without annealing. Typical TDS spectra of N_2O desorption are shown in Figure 2a. No N_2O desorption was noticed below 0.19 L (yielding the 0.7 monolayer). Above this level, the desorption showed a peak, α_1-N_2O at 140 K, and at higher exposures, α_2-N_2O at 104 K. The latter appeared after high exposures, close to saturation of N_2 desorption, and increased sharply with a further increase of

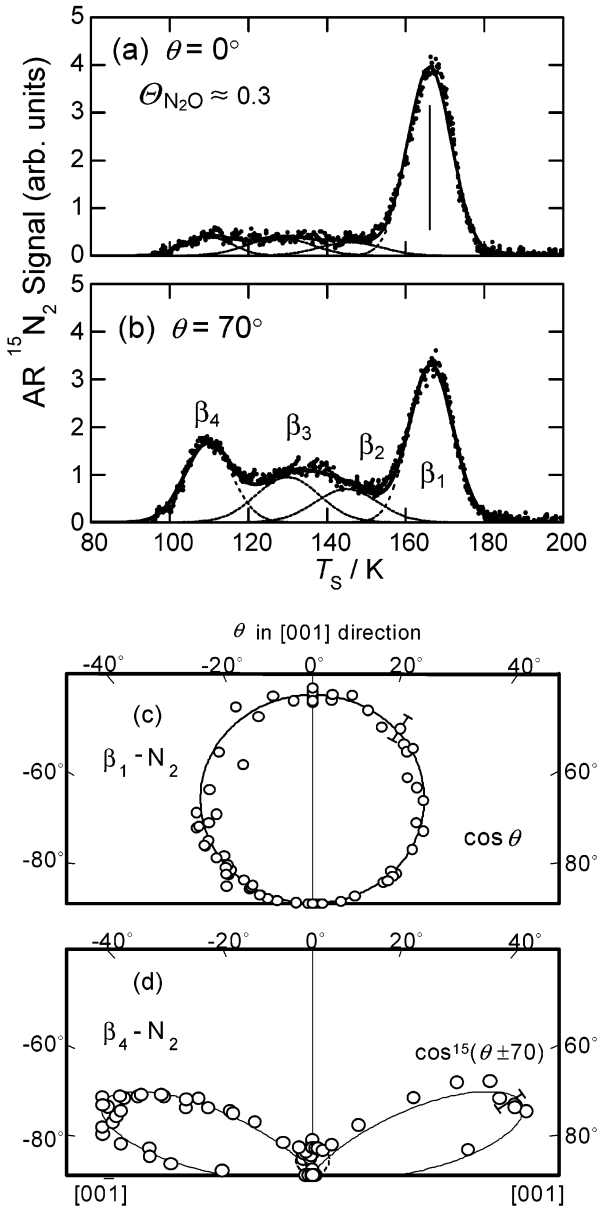

Figure 1. AR-TDS spectra of $^{15}N_2$ from $^{15}N_2O$-covered Rh(110) at $\Theta_{N_2O} = 0.3$ and at $\theta =$ (a) 0° and (b) 70°. The surface was initially clean. The heating rate was 0.6 K s^{-1}. Deconvolutions shown by dotted curves are based on a Gaussian form for each peak. The solid line indicates the sum of all the components. (c) and (d) Angular distributions of desorbing (c) β_1-N_2 at $T_S = 167$ K and (d) β_4-N_2 at $T_S = 110$ K, in the plane along the [001] direction. Error bars are also shown.

the N_2O exposure. It was assigned to desorption from the second layer.[16] The first layer was assumed to be completed by the appearance of this peak (Figure 3). This was in contrast to the clean Rh(110) on which N_2O(a) was already decomposed at the adsorption temperature around 95 K and the remaining N_2O-(a) was mostly converted into N_2(g) and O(a) in the subsequent heating. The angular distribution of α_1-N_2O showed a cosine distribution. The AR-signal level of N_2O was much lower than that of N_2.

C.2. N_2 Desorption. N_2 desorption revealed four peaks, β_1-N_2 at around 165 K, β_2-N_2 at 140 K, β_3-N_2 at 123 K, and β_4-N_2 at 105 K as shown in the AI form in Figure 2b. The AI-N_2 signal was already corrected for the contribution from the fragmentation of N_2O. As compared with the results on the clean surface, the β_1-N_2 peak was highly suppressed and showed saturation at low N_2O exposures. With increasing N_2O exposure,

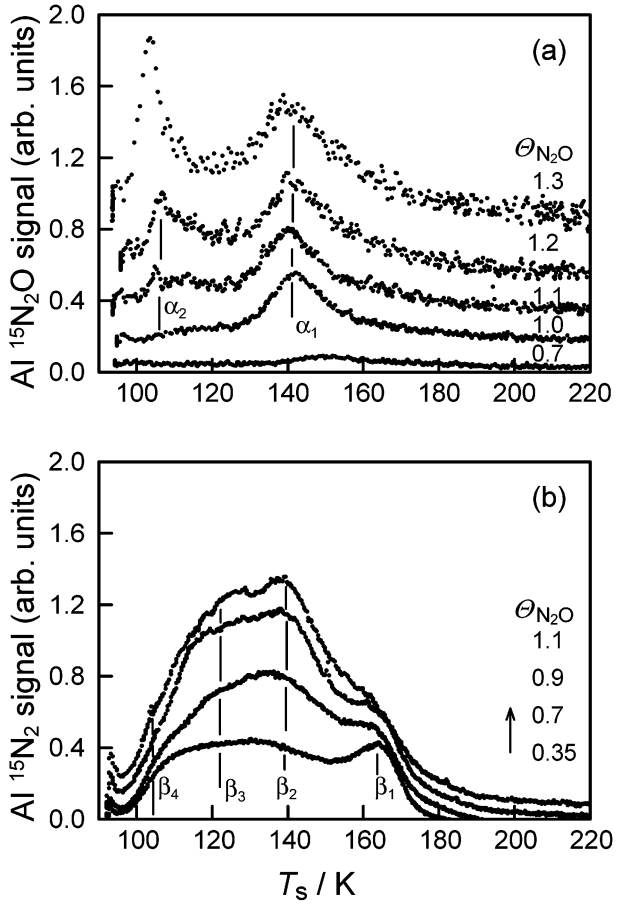

Figure 2. AI-TDS spectra of (a) $^{15}N_2O$ and (b) $^{15}N_2$ after different $^{15}N_2O$ exposures at 95 K on the oxygen-modified surface. The heating rate was 2.0 K s^{-1}.

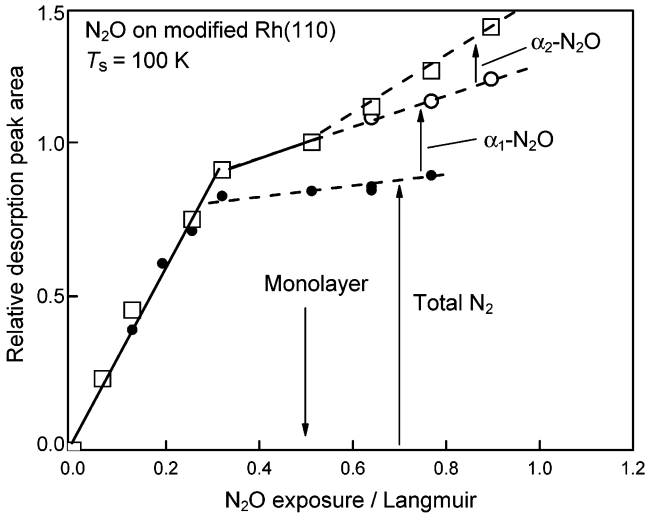

Figure 3. $^{15}N_2O$ exposure curve on the oxygen-modified surface measured by the $^{15}N_2$ and $^{15}N_2O$ desorption peak area. The $^{15}N_2$ signal from Figure 2b was plotted after subtraction of the contribution from the $^{15}N_2O$ fragmentation in the QMS in the reaction chamber, 70% of the $^{15}N_2O$ signal in the AI form.

both β_2-N_2 and β_3-N_2 increased, whereas the β_4-N_2 peak appeared as a shoulder of the β_3-N_2 peak. Here, the N_2O coverage, Θ_{N_2O}, was defined as the AI-TDS peak area relative to the sum of ($N_2 + N_2O$) at the appearance of α_2-N_2O because this α_2-N_2O can be due to desorption from the multilayer (Figure 3).

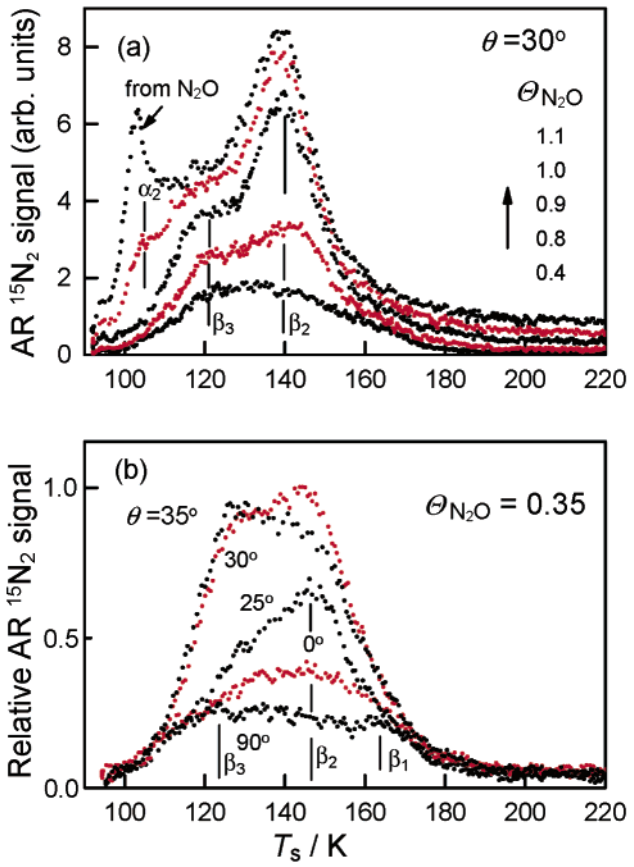

Figure 4. AR-TDS spectra of $^{15}N_2$ from the oxygen-modified Rh-(110) (a) at $\theta = 30°$ after different $^{15}N_2O$ coverages, and (b) at different θ values at $\Theta_{N_2O} = 0.35$. The heating rate was 2.0 K s^{-1}. The signals are shown without being subtracted from the contribution due to the $^{15}N_2O$ fragmentation as explained in the text. The peak at 105 K is due to the fragmentation of α_2-N_2O.

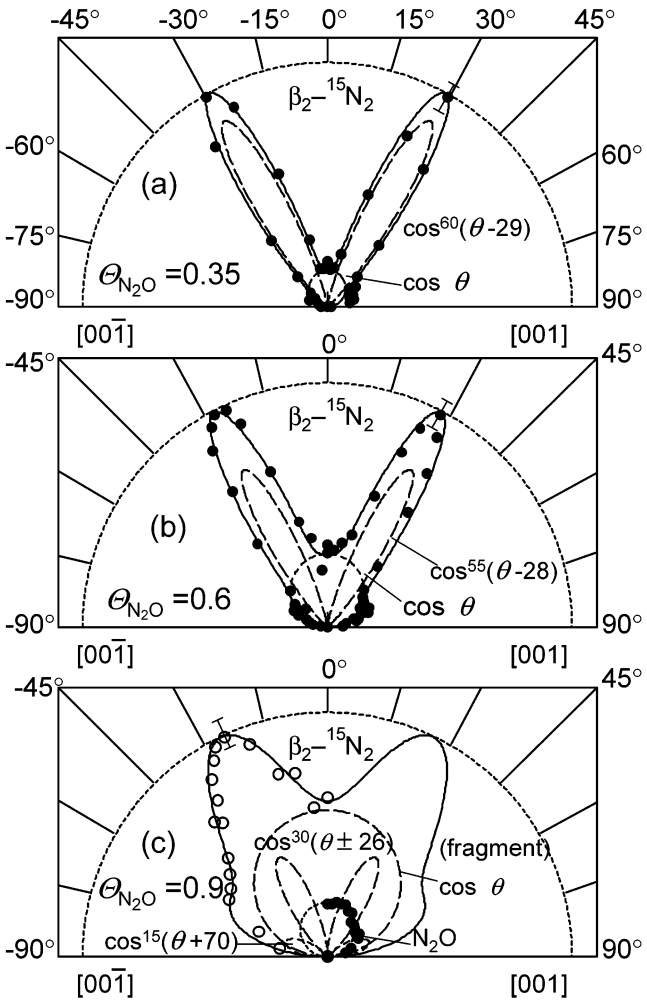

Figure 5. Angular distributions of desorbing β_2-$^{15}N_2$ in the plane along the [001] direction. Θ_{N_2O} = (a) 0.35, (b) 0.6, and (c) 0.9. The distributions in (a) and (b) were deconvoluted into two inclined components and a cosine form, as shown by broken curves. The solid lines indicate their summations. In (c) also, the angular distribution of N_2O is shown. The distribution of N_2 was deconvoluted into five components (see text). The cosine component is mostly due to the $^{15}N_2O$ fragmentation in the analyzer.

The AR-signal of N_2 was sensitive to the N_2O exposure and the desorption angle although it contained a large contribution from the fragmentation of N_2O in the analyzer. Typical AR-N_2 spectra at $\theta = 30°$ are shown at various N_2O coverages in Figure 4a, since the signal was enhanced around this angle except for low coverages. The β_2-N_2 peak at 140 K was enhanced above $\Theta_{N_2O} = 0.35$. The sharp α_2-N_2 peak appearing at around 105 K is due to the fragmentation of α_2-N_2O. Both β_2-N_2 and β_3-N_2 appeared in the whole range of the exposure. β_1-N_2 became significant at around $\theta = 0°$.

The AR-TDS shape changed sharply depending on the desorption angle (Figure 4b). This change is merely due to the angular distribution of desorbing N_2 because the fragmentation from N_2O contributes in a cosine form. It should be noted that there is a significant signal intensity at the desorption angle $\theta = 90°$. This is due to N_2 and N_2O molecules that did not pass through the slits directly from the surface but first desorbed into the reaction chamber and then penetrated the analyzer chamber. This extraneous signal was subtracted from the observed intensity for angular distribution plots. The apparatus was originally designed for the angle-resolved measurements of desorbing CO_2.[14] The pumping rate for CO_2 was about 2 m^3 s^{-1}, high enough to reduce the CO_2 penetration from the reaction chamber to a negligible level. On the other hand, the pumping rate for N_2 was estimated to be around one twentieth of that for CO_2. This pumping rate of the reaction chamber was not high enough to suppress the penetration of N_2 scattered on the reaction chamber wall to a negligible level.[17]

C.3. N_2 Angular Distribution. N_2 desorption in β_2-N_2 and β_3-N_2 revealed sharp and inclined emission collimated at around ±30°, whereas β_1-N_2 showed a cosine distribution. Each AR−N_2 spectrum was deconvoluted into four Gaussian peaks as exemplified in Figure 1,[5] and the resultant signal intensity was plotted against the desorption angle. Figure 5 shows the angular distributions of β_2-N_2 at different N_2O coverages. Except for high coverages, the angular distributions could be fitted into three desorption components, i.e., a cosine component and two symmetrically inclined components, as shown by broken curves. The solid curve in Figure 5a indicates the total N_2 flux at $\Theta_{N_2O} = 0.35$ calculated as $0.89\ \{\cos^{60}(\theta + 29) + \cos^{60}(\theta - 29)\} + 0.13\cos(\theta)$. The pre-factors indicate the relative signal intensity at this coverage. At $\Theta_{N_2O} = 0.6$, its desorption intensity was described as $0.73\ \{\cos^{55}(\theta + 28) + \cos^{55}(\theta - 28)\} + 0.3\cos(\theta)$ (Figure 5b). At $\Theta_{N_2O} = 0.9$, by considering the enhanced signal at around 70°, the total signal was approximated as $0.45\{\cos^{30}(\theta + 26) + \cos^{30}(\theta - 26)\} + 0.18\{\cos^{15}(\theta + 70) + \cos^{15}(\theta - 70)\} + 0.6\cos(\theta)$ (Figure 5c).

The angular distribution of β_3-N_2 was also examined after deconvolution. The results for $\Theta_{N_2O} = 0.6$ at 123 K are shown in Figure 6. The desorption intensity was approximated as

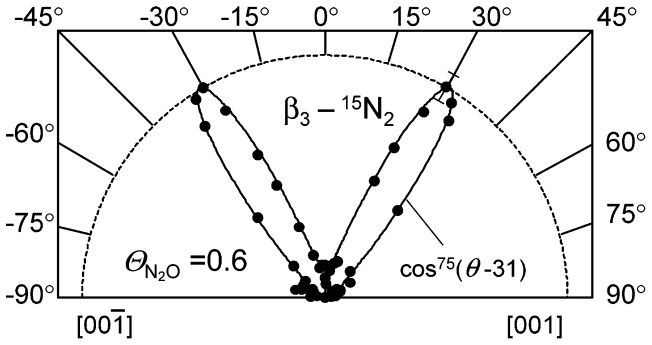

Figure 6. Angular distributions of desorbing β_3-$^{15}N_2$ in the plane along the [001] direction. $\Theta_{N_2O} = 0.6$.

$\cos^{75}(\theta + 31) + \cos^{75}(\theta - 31)$. The collimation angle was estimated to be $\theta = 31°$.

The observed AR-N_2 signal involved the contribution from the fragmentation of N_2O in the analyzer. This contribution was estimated to be 3 times higher than that of N_2O. The cosine component in Figure 5 was mostly removed by this correction (see Figure 5c) because both α_1-N_2O and β_2-N_2 peaked in the same temperature range and α_1-N_2O showed only a simple cosine distribution, while β_2-N_2 consisted of three components, i.e., a cosine component and two inclined components. After subtracting the N_2 intensity contribution from the fragmentation at $\Theta_{N_2O} = 0.9$, only the inclined components remained in the angular distribution. A similar contribution to the cosine component was confirmed at $\Theta_{N_2O} = 0.35$ and 0.6. In the β_3-N_2 case (Figure 4a), the cosine component, when present, was small. Its peak position was different from that for N_2O desorption.

D. Oxygen-Covered Rh(110). The shape of the N_2 desorption spectra was strongly affected by the preheating temperature, CO treatment, and oxygen preexposure, indicating that the presence of surface oxygen plays an important role in inducing inclined N_2 desorption.

The removal of reactive surface oxygen enhanced the β_1-N_2 formation and suppressed the formation of β_2-N_2 and β_3-N_2. The surface was first preheated at 1000 K, then CO was dosed at 100 K, and the surface was heated to 700 K. This procedure partly removed the remaining surface oxygen as CO_2.[18] The N_2 desorption spectra depended on the amount of CO exposure (Figure 7a). N_2 desorption showed only two small peaks of β_2-N_2 and β_3-N_2 without CO treatment. With increasing CO exposure, the β_1-N_2 peak appeared at around 165 K and was enhanced. The spectrum at 0.54 L CO mostly recovered the formation of β_1-N_2. This CO exposure was considered to be large enough to remove most of the residual surface oxygen.

Similar changes in the N_2 TDS spectra were also found by prolonged heating of the sample (Figure 7b). The N_2 spectrum with two peaks in a similar intensity was observed after 0.16 L N_2O exposure without keeping the preheating temperature at 1000 K. With an increasing heating period at 1000 K, the β_1-N_2 peak was largely recovered. However, the β_2-N_2 and β_3-N_2 peaks were still significant even after 6 min of heating. Prolonged heating at 1000 K was not enough to remove the surface oxygen.[9]

The N_2 desorption was largely suppressed when the surface was pre-covered by oxygen. It decreased quickly with increasing oxygen pre-coverage and was mostly suppressed at 0.1 L O_2. This exposure can yield surface oxygen to about 0.1 monolayer because of the sticking probability close to unity.[9] It should be noticed that a small amount of surface oxygen can kill active sites for the N_2O decomposition, but the remaining oxygen after annealing at 1100 K does not. Instead the remaining oxygen modifies the N_2 desorption.

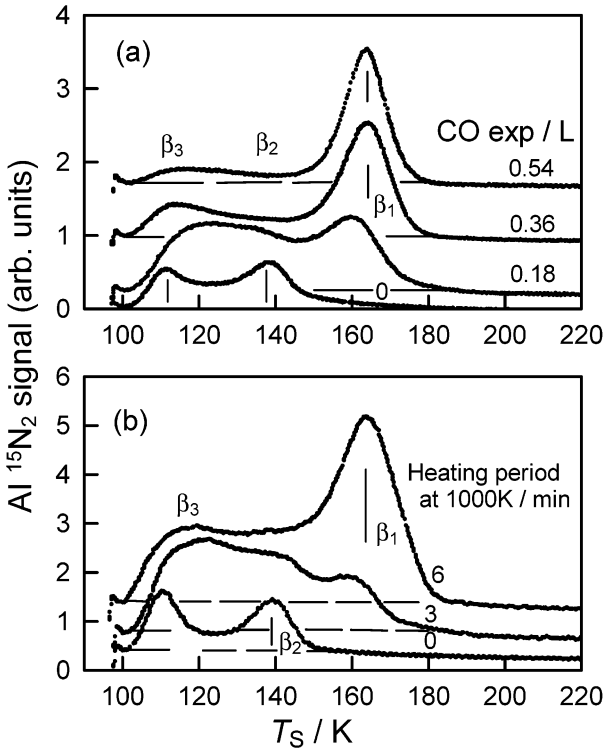

Figure 7. TDS spectra of $^{15}N_2$ from $^{15}N_2O$-covered Rh(110) prepared in different ways. The surface was exposed to 0.16 L of N_2O at 105 K (a) after treatment with CO at different exposures at 200 K, causing the residual surface oxygen to be removed by being heated, and (b) with different annealing periods at 1000 K.

IV. Discussion

A. N_2 Desorption Components. N_2O decomposition yielded four N_2 desorption peaks in the range of 100−180 K. β_1-N_2 showed a cosine distribution, being consistent with the desorption from the adsorption state of N_2. The peak temperature of 160−165 K agrees well with that of desorption of N_2(a) on the clean Rh(110). The N_2(a) formation may proceed below the desorption temperature of β_1-N_2 (150−180 K) as $N_2O(a) \rightarrow N_2(a) + O(a)$. This cosine component was estimated to contribute about 70% of the total amount of desorbing N_2 on the clean surface at low N_2O coverage. On the modified surface, this cosine component was relatively reduced to below 20%. Concomitantly, the β_2-N_2 and β_3-N_2 peaks were enhanced. These peaks as well as β_4-N_2 are due to direct desorption from the N_2O(a) decomposition events because of their sharp angular distributions. The differences in the peak temperature were due to different activation energies of N_2O(a) decomposition. β_4-N_2 desorption was sharply collimated at around 70°. This 70° component was not clearly separated on the modified surface. It peaked at around 110 K, showing the smallest activation energy. This 70° component may also be involved in both β_2-N_2 and β_3-N_2 on the modified surface as expected from the results on the clean surface, however, it was noticed only at high coverages (Figure 5c). β_3-N_2 and β_2-N_2 peaking at 115 and 140 K, respectively, need higher activation energies. The activation energy increases with an increasing amount of O(a) probably because of the decreasing number of vacant sites and the stabilizing effect toward the N_2O(a).[19] The small amount of surface oxygen is known to increase the heat of adsorption of N_2O on Ru(001).[24] The adsorption site becomes somewhat

electron-deficient by the modification caused by adsorbed oxygen with a high electronegativity, and N_2O is more stabilized in the form interacting with metal as an electron donor through a 7σ nonbonding orbital localized on the terminal nitrogen atom. Thus, the deposition of oxygen during N_2O dissociation may shift the decomposition temperature upward.

B. Surface Structure. The clean Rh(110) surface is stable in the (1×1) form without reconstruction. The surface is reconstructed into missing-row forms with $(1 \times n)$ periodicity when it is covered by oxygen. The missing-row structure with half a monolayer of oxygen, a (2×2)p2mg lattice that is stabilized by oxygen, is converted into the (1×1) form above about 500 K after removal of oxygen by the reaction with CO or hydrogen.[20] The missing-row surface consists of terraces with a (111) structure declining alternatively about $+35°$ and $-35°$ in the [001] direction. Recent STM work indicates that oxygen in the (2×2)p2mg lattice forms O−Rh−O−Rh zigzag chains extending along the $[1\bar{1}0]$ direction.[10] It is difficult to consider N_2O dissociation on the (2×2)p2mg lattice because the local oxygen coverage is half a monolayer and no N_2O dissociation takes place above about 0.1 monolayer without annealing. The surface preheated at 1100 K was estimated to be covered by oxygen at the relative coverage of 0.20.[9] Thus, the present modified surface is partly covered by either the (1×1) or (1×2) facets, which is consistent with LEED results.

C. N_2O Structure. N_2O(a) was proposed to adsorb via its terminal N atom on metal surfaces in an upright standing form or in an inclined one.[16,21−24] Prior to decomposition, however, N_2O must lie to release oxygen on the surface. Thus, the decomposition of N_2O aligned in the [001] direction was first proposed as the decomposition precursor on Pd(110)(1×1).[4] A recent density-functional theory (DFT) calculation with a generalized gradient approximation by Kokalj[25,26] shows that the parallel form of N_2O on Pd(110) is in a bending configuration, bridging atomic Pd troughs extending in the $[1\bar{1}0]$ direction. It is as stable as a standing or tilting form with bonding via the terminal nitrogen atom to the surface. Recent near-edge X-ray absorption fine-structure spectroscopy (NEXAFS) measurements of N_2O on Pd(110) at around 60 K showed remarkable anisotropy in the X-ray polarization dependence of the two π resonance (N 1s → $3\pi^*$) NEXAFS peaks at 401 and 405 eV of the photon energy.[15] This is consistent with the dominance of [001]-oriented N_2O(a). A similar adsorbed N_2O molecule was also predicted on Rh(110)(1×1) by DFT calculations.[27]

On the other hand, no N_2O dissociation is expected on the (1×2) part because of the presence of 0.5 monolayer of oxygen, although this possibility cannot be completely ruled out. The remaining oxygen after annealing at 1100 K may be located beneath the surface and may modify the adsorption site for N_2O.

D. N_2 Inclined Desorption. Inclined N_2 emission takes place merely from N_2O dissociation. No associative desorption of N(a) takes place on the present surface below 200 K because of the difficulty of the N−N bond scission. The repulsive desorption in thermal reactions reported so far (except for N_2O(a) decomposition) is due to the formation of bulky molecules in close proximity to the surface, i.e., Pauli repulsion is operative between the product molecule and the site. It should be noted that the N_2 desorption from the process of N(a) + N(a) → N_2(g) on Pd(110) and Rh(110) shows normally directed desorption, similarly to reactive CO_2 desorption. The surface corrugation of Rh(110)(1×1) is not large enough to induce inclined desorption. The size of CO_2 is about 3.8 Å × 5.2 Å from the van der Waals' radii, and that of N_2 is 4.0 Å × 4.0 Å. These values are close to the distance between the nearest surface rhodium atoms in the [001] direction, 3.81 Å. In fact, the inclined desorption of CO_2 becomes possible on a somewhat wider (three-atom-wide) terrace (about 4.76 Å).[28] For the inclined N_2 desorption from N_2O(a) decomposition on flat (1×1) planes, therefore, additional factors must be invoked.

The direction of N_2 desorption is controlled by the balance between the repulsive (or attractive) forces from surface rhodium atoms and those from nascent oxygen with high energy. The latter force is a principal factor. The dissociation is completed by breaking the N_2−O bond, emitting N_2. The product N_2 receives a repulsive force mostly from the nascent oxygen along the ruptured N−O bond immediately after N_2O dissociation. For the 70° component, the N_2O being dissociated must be in a form close to the surface parallel and oriented along the [001] direction because repulsions operative closely parallel to the surface plane are only possible from the nascent oxygen atom. On the other hand, for the 30° component, the interaction from rhodium atoms becomes weaker than that for the 70° component, i.e., only the repulsive force from the nascent oxygen atom is operative. The N_2 collimation will be determined solely by the angle population of the inclined transient N_2O. A highly inclined N_2O(a) interacting *with metal by the oxygen atom* is invoked although such an adsorption structure has never been proposed on noble metals. The transient N_2O molecule must be inclined at around the collimation angle, i.e., about 30°. Such inclined N_2O is predicted to be formed on the site modified by oxygen. This modified site is different from that in the above model to stabilize N_2O(a) by adsorbed surface oxygen. The involved O(a) does not block the N_2O(a) adsorption but rather enhances the adsorption of tilted N_2O adsorbed via its oxygen atom to the surface.

E. Comparison with the Other Surfaces. Desorbing β_1-N_2 on Pd(110), which is described as $\cos^{50}(\theta + 43) + \cos^{50}(\theta - 43)$, possesses a high kinetic energy (about 45 kJ mol^{-1}). Both β_2-N_2 as $\cos^{30-60}(\theta + 28) + \cos^{30-60}(\theta - 28)$ and β_3-N_2 as $\cos^{75}(\theta + 30) + \cos^{75}(\theta - 30)$ on Rh(110) show similar sharpness of distribution and collimation angles close to the value on Pd(110). On the other hand, β_4-N_2 shows a broader distribution and larger collimation angles in a form of $\cos^{15}(\theta + 70) + \cos^{15}(\theta - 70)$.

A higher translational energy is expected for molecules with sharper angular distributions, although the translational energy generally depends on the surface crystal azimuth. Both β_2-N_2 and β_3-N_2 on Rh(110) are expected to show higher energy than that on Pd(110) because of the sharper angular distributions. During stabilization of the nascent product O(a) in N_2O dissociation, a large amount of the energy due to the O−metal bonding must be dissipated; the available energy which the product can carry out, ΔE_T, is given as, $\Delta E_T = E_{N_2(g)} + E_{O(a)} - E_{N_2O(a,TS)}$, where $E_{N_2(g)}$, $E_{O(a)}$, and $E_{N_2O(a,TS)}$ are the potential energies of N_2(g), O(a), and the transition state of N_2O(a) dissociation, respectively. By assuming 400−500 kJ mol^{-1} as the bond energy of O−metal,[29] the available energy was estimated to be 240−340 kJ mol^{-1}, because the dissociation[30] of $N_2O(g) \rightarrow N_2(g) + O(g)(^3P)$ is endothermic of about 160 kJ mol^{-1}, and the heat of adsorption of N_2O on both Pd(110) and Rh(110) is close to the activation energy of N_2O(a) dissociation. Thus, the emitted energy mostly comes from the metal−O bond formation. The nascent oxygen may transfer a momentum toward nascent N_2 along the ruptured N−O bond.

This hot-atom-assisted model predicts that the translational energy on Rh(110) is higher than that on Pd(110) because more energy is expected to be released, although no reliable experimental data are found for the heat of adsorption of oxygen on

Pd(110) and Rh(110), i.e., the angular distribution on Pd(110) must be broader than that on the others. In this case, the sharpness of the angular distribution of β_2-N_2 and β_3-N_2 on the oxygen-modified surface may be compared with the results on Pd(110), whereas β_4-N_2 on the clean surface collimated close to the surface parallel is likely to be affected by scattering on the surface. This model can be examined by velocity measurements or state-selective desorption measurements.[31]

V. Summary

The decomposition of N_2O(a) on Rh(110) proceeded at 100−180 K and yielded four N_2 desorption peaks, at around 110 K (β_4-N_2), 120−130 K (β_3-N_2), 140−150 K (β_2-N_2), and 160−165 K (β_1−N_2). The appearance of these peaks depended on the N_2O coverage and the annealing after oxygen adsorption. The β_1-N_2 peak showed a cosine distribution and was assigned from the desorption of adsorbed N_2. On the other hand, β_2-N_2 and β_3-N_2 on the oxygen-modified surface revealed inclined and sharp collimation at around 30° off the surface normal, and β_4-N_2 was observed on the oxygen-free surface and collimated at around 70° off the normal, close to the [001] direction. An N_2 desorption mechanism was proposed on the clean (1×1) and oxygen-modified surfaces, where the decomposition of N_2O(a) inclined or aligned along the [001] direction induces the inclined desorption.

Acknowledgment. Suwen Liu acknowledges the support he received from the Ministry of Education, Science, Sports and Culture of Japan through the foreign-researcher (COE) invitation program in 2000−2001. Izabela Rzeźnicka is indebted to the above Ministry for her 2000−2004 scholarship. Anton Kokalj and Ivan Kobal were supported by the scientist-exchange program between the Japanese Society for the Promotion of Science (JSPS) and the Ministry of Education, Science, and Sports of Slovenia in 2002. This work was partly supported by Grant-in-Aid No. 13640493 for General Scientific Research from JSPS.

References and Notes

(1) Pârvulescu, V. I.; Grange, P.; Delmon, B. *Catal. Today* **1998**, *46*, 233.

(2) Campbell, C. T.; White, J. M. *Appl. Surf. Sci*. **1978**, *1*, 347.

(3) Kobal, I.; Kimura, K.; Ohno, Y.; Matsushima, T. *Surf. Sci*. **2000**, *445*, 472.

(4) Ohno, Y.; Kimura, K.; Bi, M.; Matsushima, T. *J. Chem. Phys*. **1999**, *110*, 8221.

(5) Horino, H.; Liu, S.; Hiratsuka, A.; Ohno, Y.; Matsushima, T. *Chem. Phys. Lett*. **2001**, *341*, 419.

(6) Ikai, M.; Tanaka, K. I. *J. Phys. Chem. B* **1999,** *103*, 8277.

(7) Matsushima, T. *Catal. Surv. Jpn*. **2002**, *5*, 71.

(8) Comelli, G.; Dhanak, V. R.; Kiskinova, M.; Prince, K. C.; Rosei, R. *Surf. Sci. Rep*. **1998**, *32*, 165.

(9) Schwarz, E.; Lenz, J.; Wohlgemuth, H.; Christmann, K. *Vacuum* **1990**, *41*, 167.

(10) Vesselli, E.; Africh, C.; Baraldi, A.; Comelli, G.; Esch, F.; Rosei, R. *J. Chem. Phys*. **2001**, *114*, 4221.

(11) Horino, H.; Rzeźnicka, I.; Kokalj, A.; Kobal, I.; Hiratsuka, A.; Ohno, Y.; Matsushima, T. *J. Vac. Sci. Technol. A* **2002**, *20*, 1592.

(12) Belton, D. N.; DiMaggio, C. L.; Schmieg, S. J.; Simon Ng, K. Y. *J. Catal*. **1995**, *157*, 559.

(13) Zaera, F.; Gopinath, C. S. *Chem. Phys. Lett*. **2000**, *332*, 209.

(14) Matsushima, T. *Surf. Sci*. **1983**, *127*, 403.

(15) Horino, H.; Rzeźnicka, I.; Matsushima, T.; Takahashi, K.; Nakamura, E. *UVSOR Activity Report 2002*; Institute for Molecular Science, 2003; pp 209, 211.

(16) Avery, N. R. *Surf. Sci*. **1983**, *131*, 501.

(17) Kobayashi, M.; Tuzi, Y. *J. Vac. Sci. Technol*. **1979**, *16*, 685.

(18) Matsushima, T.; Ohno, Y. *Catal. Lett*. **1994**, *23*, 313.

(19) Huang, H. H.; Seet, C. S.; Zou, Z.; Xu, G. Q. *Surf. Sci*. **1996**, *356*, 181.

(20) Dhanak, V. R.; Comelli, G.; Cautero, G.; Paulucci, G.; Prince, K. C.; Kiskinova, M.; Rosei, R. *Chem. Phys. Lett*. **1992**, *188*, 237.

(21) Cornish, J. C. L.; Avery, N. R. *Surf. Sci*. **1990**, *235*, 209.

(22) Väterlein, P.; Krause, T.; Bässler, M.; Fink, R.; Umbach, E.; Taborski, J.; Wüstenhagen, V.; Wurth, W. *Phys. Rev. Lett*. **1996**, *76*, 4749.

(23) Haq, S.; Hodgson, A. *Surf. Sci*. **2000**, *463*, 1.

(24) Umbach, E.; Menzel, D. *Chem. Phys. Lett*. **1981**, *84*, 491.

(25) Kokalj, A.; Kobal, I.; Horino, H.; Ohno, Y.; Matsushima, T. *Surf. Sci*. **2002**, *506*, 196.

(26) Kokalj, A.; Kobal, I.; Matsushima, T. *J. Phys. Chem. B* **2003**, *107*, 2741.

(27) Kokalj, A.; Kobal, I.; Imamura, K.; Horino, H.; Rzeźnicka, I.; Matsushima, T. *Abstract of ECOSS-22* **2003**, No. 17006.

(28) Matsushima, T. *Heterog. Chem. Rev*. **1995**, *2*, 51.

(29) Brown, W. A.; Kose, R.; King, D. A. *Chem. Rev*. **1998**, *98*, 797.

(30) Ross, S. K.; Sutherland, J. W.; Kuo, S.-C.; Klemm, R. B. *J. Phys. Chem. A* **1997,** *101*, 1104.

(31) Hodgson, A. *Prog. Surf. Sci*. **2000**, *63*, 1.